Refined Annotations and Specialized Augmentation for Minor Epicardial Arteries in Coronary Angiography

Do-Hyun Kim[+1,2], Sangwoo Moon[+3], Dae-Hyeon Choe[4], Je Yoon Shin[5], Su-Jin Kim[6], Jae Jin Lee[7], DaeHong Kang[8], Jihwan Moon[9], and Si-Hyuck Kang[1,2,*]

[1]Cardiovascular Center, Seoul National University Bundang Hospital, Seongnam-si, Republic of Korea
[2]Department of Internal Medicine, Seoul National University, Seoul, Republic of Korea
[3]Department of Computer Science and Engineering, Seoul National University, Seoul, Republic of Korea
[4]Interdisciplinary Program of Medical Informatics, Seoul National University College of Medicine, Seoul, Republic of Korea
[5]Department of Internal Medicine, Seoul National University Hospital, Seoul National University College of Medicine, Seoul, Republic of Korea
[6]Department of Family Medicine, Seoul National University Hospital, Seoul, Republic of Korea
[7]Department of Urology, Seoul National University Hospital, Seoul National University College of Medicine, Seoul, Republic of Korea
[8]Seoul National University Hospital, Seoul, Republic of Korea
[9]Interdisciplinary Program in Artificial Intelligence, Seoul National University, Seoul, Republic of Korea
[+]The first two authors contributed equally to the manuscript
[*]eandp303@snu.ac.kr

ABSTRACT

AI-based analysis of coronary angiography (CAG) has advanced rapidly in recent years. However, the number of public CAG datasets remains limited, and existing datasets often exclude small vessels because they are not primary treatment targets and their annotation is technically challenging. Further progress in CAG segmentation requires both larger datasets and precise labeling of small-caliber vessels. We developed a CAG segmentation framework that incorporates refined annotations, CAG-specific augmentation, and a small-vessel-focused evaluation metric. The refined dataset (Fine-ARCADE dataset) comprises 196 right coronary artery images with additional annotations of minor epicardial arteries. Copy-paste augmentation was modified for vessel images by matching intensities, adjusting vessel overlap, and varying branching complexity to enhance data diversity. We fine-tuned SAM-Med2D model on public and augmented CAG datasets for 50 epochs. Segmentation performance was evaluated using three metrics: $\text{Dice}_{\text{overall}}$ (full vessel tree), $\text{Dice}_{\text{minor}}$ (minor epicardial arteries), and $\text{Dice}_{\text{major}}$ (major epicardial arteries). Fine-tuned models outperformed the pretrained baseline across all public CAG datasets. CAG-specific augmentation significantly improved $\text{Dice}_{\text{overall}}$ by up to 8.95% and $\text{Dice}_{\text{minor}}$ by up to 12.17%, with the best gains observed in the ARCADE and XCAD datasets. These results suggest that while existing public CAG datasets provide limited assessment of small-vessel segmentation, refined annotations enabled more accurate evaluation, and CAG-specific augmentation effectively enhances model performance in minor epicardial regions.

Introduction

Coronary angiography (CAG) is a standard diagnostic technique for imaging the coronary arteries[1,2]. However, visual estimation of stenosis severity by operators is highly variable between observers and even within observers, thereby limiting reproducibility[3]. Objective analysis methods, including quantitative coronary angiography (QCA) and the SYNTAX score, have been developed to provide a more structured assessment of lesion complexity[4–6]. More recently, fractional flow reserve (FFR) estimation based on three-dimensional QCA has emerged as a compelling alternative to invasive wire-based FFR measurement[7,8]. These technologies rely on proprietary algorithms for essential tasks such as contour detection, centerline extraction, reference segment identification, and calculation of key variables.

A significant limitation of conventional QCA and angiography-based FFR is their dependence on human input – operators need to select optimal image angles and best frames, and often need to correct vessel contours and diseased segments. Recent advances in artificial intelligence (AI) offer the potential to automate this lesion assessment, thereby saving human time and

effort[9–11]. Segmentation is the key step for any AI-based analysis of CAG. Despite AI's success in other segmentation tasks, its application to CAG remains limited.

Challenges in CAG Segmentation

While segmenting medical images requires specialized domain knowledge, CAG poses additional challenges, including diverse coronary anatomy variants, vessel tortuosity, overlapping vessels in 2D, and complex microvasculature. This problem is compounded by a scarcity of public datasets and segmentation labels[12]. Existing segmentation labels are often coarse, focusing mainly on major epicardial arteries and excluding the smaller microvessels[13–15]. Minor epicardial arteries, such as the sinus node artery, conus branch, acute marginal branches, and septal branches, are often omitted because of their small caliber and poor delineation on CAG, which makes annotation more challenging. Therefore, it is important to explore alternative strategies to enhance the segmentation of minor epicardial arteries by leveraging major epicardial arteries.

The coronary arterial circulation comprises both large epicardial arteries and a smaller microvascular system[16]. While only epicardial coronary arteries are visualized by CAG, most segmentation tasks focus on major large epicardial segments with diameters of 2 mm or greater. The microvascular system, including prearterioles and intramural arterioles, although not well-delineated on angiography, is crucial for maintaining coronary perfusion pressure and myocardial blood supply. Minor epicardial arteries with smaller diameters ranging from 500 μm to 2 mm are responsible for distributing blood throughout the myocardium with minimal resistance.

The focus on large epicardial arteries is often justified because vessels with a diameter greater than 2 mm are the primary targets for coronary interventions, such as balloon angioplasty or stent implantation. However, the coronary artery system of the heart is a complex vascular structure that resembles a tree. Analysis of smaller vessels, such as those less than 2 mm in diameter, may provide a comprehensive understanding of coronary anatomy and blood flow. This is particularly relevant at bifurcations, where vessel diameters change abruptly and hemodynamics are notoriously complex to model[17,18]. Furthermore, coronary microvascular dysfunction is gaining clinical attention due to its prevalence, impact on patient outcomes, and diagnostic and therapeutic challenges[19].

Our Contributions

This study aims to leverage a low-quality, coarse-labeled dataset to train a high-quality segmentation model that accurately delineates vessels down to the level of small, traceable vessels. Our main contributions are as follows.

1. **Fine-labeled High-Quality Evaluation Dataset:** We propose a novel, physician-refined evaluation dataset, Fine-ARCADE, by re-annotating an existing coarse-labeled dataset (*i.e.*, ARCADE). This refined dataset meticulously covers both major and minor vessels, providing a reliable standard for accurate CAG segmentation assessment.

2. **Vessel Size-Specific Evaluation Metrics:** We introduce three complementary evaluation metrics—$\text{Dice}_{\text{overall}}$, $\text{Dice}_{\text{major}}$, and $\text{Dice}_{\text{minor}}$—to offer a granular assessment of model performance based explicitly on vessel size.

3. **Anatomy-Guided CAG Augmentation:** We enhance the standard Copy-Paste augmentation method by incorporating anatomical knowledge to boost CAG segmentation performance further. We experimentally validate that our proposed method consistently improves performance across three distinct low-quality training datasets[13–15].

Related works

Segment Anything Model (SAM) and SAM-Med2D

SAM is a foundation model for image segmentation[20]. It performs image segmentation using interactive prompts, such as points, bounding boxes, or masks. The interactive prompt encoder improves the model's ability to delineate complex object boundaries, enhancing segmentation accuracy. SAM was originally trained on a large-scale natural image dataset containing 11 million images and 1.1 billion masks.

Given the substantial domain gap between natural and medical images, many studies have focused on fine-tuning SAM for medical imaging applications[21–23]. **SAM-Med2D** adapts SAM to the medical domain by freezing the image encoder and inserting learnable adapter layers into each transformer block to capture medical-specific knowledge[24]. The prompt encoder and mask decoder were fine-tuned, with later iterations updating only the mask decoder. The model was trained on a dataset composed of 4.6 million medical images and 19.7 million masks. This combination of architectural adaptation and large-scale training significantly improved segmentation performance on medical images. It achieved high accuracy even with a single-point prompt and allowed more efficient user interaction. Given its strong performance in medical image segmentation, SAM-Med2D was selected as the baseline model for CAG segmentation in our study. In this study, we use SAM-Med2D for CAG segmentation.

Public CAG Datasets

The public CAG datasets with available segmentation masks are summarized in Table 1[13–15]. The ARCADE dataset[13] is a public benchmark composed of 1,500 single-frame coronary angiography images and their corresponding vessel segmentation masks. The annotated vessels are labeled according to the coronary artery classification defined by the SYNTAX score. The XCAD[14] and DCA1[15] datasets do not provide detailed protocols for manual labeling, but the ground truth annotations were created by expert radiologists and an expert cardiologist, respectively. While these datasets have served as key resources in previous studies, their annotations are largely limited to major arteries, and minor arteries remain unlabeled. Training models without detailed ground-truth datasets not only leads to insufficient segmentation performance in minor artery regions but also renders them inadequate as precise evaluation tools for CAG segmentation. To overcome these significant limitations, there is a need for advanced training methods specifically designed to address data sparsity in minor arteries, alongside the establishment of an appropriate benchmark to accurately assess minor artery segmentation performance.

Copy-Paste Augmentation

Copy-Paste augmentation is a technique that generates new training samples by pasting segmented objects from a source image onto a target (background) image[25]. It has proven effective in natural image tasks by increasing object diversity and scale variation while requiring minimal computational resources. However, applying Copy-Paste augmentation directly to CAG segmentation is challenging. CAG images are displayed in grayscale, making vanilla Copy-Paste difficult to apply. In addition, ignoring the fractal geometry of the coronary artery tree can lead to unrealistic vascular structures[26].

Methods

This section introduces the Standard Copy-Paste augmentation technique, presents our proposed method (Modified Augmentation Techniques for CAG), and provides the corresponding pseudo-code implementation in Algorithm 1. For clarity in describing this process, we utilize the following notations throughout this paper. We assume access to two pairs of images and masks: a background pair and a foreground pair.

- **Background Image and Mask:** I_{bg} denotes the background CAG image, and M_{bg} is its corresponding vessel mask. This pair represents the existing coronary tree structure to which new vessels will be added.
- **Foreground Image and Mask:** I_{fg} denotes the foreground CAG vessel image, and M_{fg} is its corresponding vessel mask. This pair represents the vessel segment that will be copied and inserted into the background.
- **Geometric Transformation:** T denotes a geometric transformation applied to the foreground segment, including operations such as resizing and relocation.

Introduction to Standard Copy-Paste Augmentation

Standard Copy-Paste augmentation[25] synthesizes a new image by applying a **geometric transformation** (T) to a foreground object $I_{\text{fg}} \odot M_{\text{fg}}$ and its mask M_{fg} before inserting it into a background image I_{bg}. The foreground mask also undergoes the same geometric transformation and is subsequently merged with the background mask.

$$I_{\text{aug}} = T(I_{\text{fg}} \odot M_{\text{fg}}) + I_{\text{bg}} \odot (1 - T(M_{\text{fg}})) \tag{1}$$

$$M_{\text{aug}} = T(M_{\text{fg}}) + M_{\text{bg}} \odot (1 - T(M_{\text{fg}})) \tag{2}$$

Where I_{aug} is the augmented image and $\odot$ denotes element-wise multiplication.

However, applying this naively to CAG images requires three specific modifications to maintain anatomical and visual fidelity.

Modified Augmentation Techniques for CAG

Intensity Matching

This modification ensures **visual consistency** by making the sampling probability of a foreground vessel segment inversely proportional to its intensity mismatch with the background artery.

- **Representative Intensity:** The mean pixel intensity of the vessel.

$$\text{Intensity}_{\text{vessel}} = \frac{1}{|\text{Pixel}_{\text{vessel}}|} \sum_{p \in \text{Pixel}_{\text{vessel}}} p \tag{3}$$

- **Intensity Difference:** The absolute difference in representative intensities between the candidate foreground segment k and the background vessel.

$$\Delta\text{Intensity}_k = |\text{Intensity}_{\text{fg},k} - \text{Intensity}_{\text{bg}}| \tag{4}$$

- **Normalized Sampling Probability:** Prioritizes segments with smaller $\Delta\text{Intensity}_k$. M is the total number of candidates, and $W_k = f(\Delta\text{Intensity}_k)$ is an inverse function. (e.g., $W_k = 1/(\Delta\text{Intensity}_k + \varepsilon)$).

$$P_{\text{sample},k} = \frac{W_k}{\sum_{j=1}^{M} W_j} \tag{5}$$

Overlapped Vessels

This modification ensures **anatomical continuity** by enforcing a connection between the new vessel segment and the existing coronary tree structure.

- **Description:** A geometric transformation is sought that guarantees an **Overlap** between the transformed foreground vessel and a suitable background vessel. Once the connection is established, blending is performed.

- **Connection Condition:** A valid connection exists if the Overlap() is strictly greater than zero for some transformation. The Overlap() function returns the count of overlapping pixels between two masks.

$$\exists T \text{ such that } \text{Overlap}(T(M_{\text{fg}}), M_{\text{bg}}) > 0 \tag{6}$$

Multiple Insertion

This modification captures the **fractal geometry and complexity** of the coronary artery tree by sequentially increasing the number of branches.

- **Description:** The complete augmentation process is repeated N times. The outputs from the previous step (I_{i-1}, M_{i-1}) serves as the background fo the current step ($I_{bg,i}$, $M_{bg,i}$).

- **Sequential Insertion:**

$$I_{\text{aug,i}} = T(I_{\text{fg,i}} \odot M_{\text{fg,i}}) + I_{\text{bg,i}} \odot (1 - T(M_{\text{fg,i}})) \tag{7}$$

$$M_{\text{aug,i}} = T(M_{\text{fg,i}}) + M_{\text{bg,i}} \odot (1 - T(M_{\text{fg,i}})) \tag{8}$$

  Where $I_0 = I_{\text{bg}}$, $M_0 = M_{\text{bg}}$ and the final augmented image and mask are $I_{\text{final}} = I_{aug,N}$. $M_{\text{final}} = M_{aug,N}$.

Fine-tuning SAM-Med2D with Public and Augmented CAG Datasets

We fine-tuned SAM-Med2D using both public CAG datasets and their augmented versions described in Section 3.2. We applied a single-point prompt method for the prompt encoder. The same hyperparameters as in the original SAM-Med2D training were applied, except for the number of training epochs. Training was run for 50 epochs instead of the default setting to ensure sufficient convergence for CAG segmentation.

Evaluation

We conducted all evaluations on the Fine-ARCADE dataset. Segmentation performance was evaluated for each training dataset and for the pretrained SAM-Med2D model using the Dice similarity coefficient. We reported three variants of the Dice similarity coefficient metric reflecting different regions of the coronary tree. $\text{Dice}_{\text{overall}}$ was computed against the whole ground truth, defined as the union of the original annotations and the re-annotated minor artery masks. $\text{Dice}_{\text{minor}}$ was computed only within the re-annotated minor epicardial artery masks, providing a specific assessment of segmentation performance in minor artery regions. $\text{Dice}_{\text{major}}$ was computed only within the original annotation areas, which covered the major epicardial arteries, and corresponds to the conventional evaluation metric used in prior studies. Figure 1 provides a schematic overview of the workflow described above.

Algorithm 1 CAG-specific Copy-Paste Augmentation

Require: $I_{\text{bg}}, M_{\text{bg}}$ (Background image and mask), $\mathscr{I}_{\text{fg}}, \mathscr{M}_{\text{fg}}$ (Set of foreground image and mask), $N_{\text{Insertions}}$ (Number of insertions), T (geometric transformation function)

Ensure: $I_{\text{Augmented}}, M_{\text{Augmented}}$ (Final augmented image and mask)

$I_{\text{Augmented}} \leftarrow I_{\text{bg}}$
$M_{\text{Augmented}} \leftarrow M_{\text{bg}}$
$\text{Intensity}_{\text{bg}} \leftarrow \text{CalculateMeanIntensity}(I_{\text{Augmented}}, M_{\text{Augmented}})$
$\mathscr{P}_{\text{sample}} \leftarrow \text{CalculateNormalizedProbabilities}(\mathscr{I}_{\text{fg}}, \mathscr{M}_{\text{fg}}, \text{Intensity}_{\text{bbg}})$
for $i = 1$ TO $N_{\text{Insertions}}$ **do**
  // Intensity Matching (Eq. 3-5)
  $(I_{\text{fg}}, M_{\text{fg}}) \leftarrow \text{SampleForeground}(\mathscr{P}_{\text{sample}})$
  // Overlap and Seamless Merging (Eq. 6: Connection Check)
  if $\text{Overlap}(T(M_{\text{Seg}}), M_{\text{Augmented}}) > 0$ **then**
    // Multiple Insertion (Eq. 7, 8: Sequential Copy-Paste)
    $I_{\text{Augmented}} \leftarrow T(I_{\text{fg}} \odot M_{\text{fg}}) + I_{\text{Augmented}} \odot (1 - T(M_{\text{fg}}))$
    $M_{\text{Augmented}} \leftarrow T(M_{\text{fg}}) + M_{\text{Augmented}} \odot (1 - T(M_{\text{fg}}))$
  else
    CONTINUE {Try next iteration}
  end if
end for
RETURN $I_{\text{Augmented}}, M_{\text{Augmented}}$

Results

Figure 2 visualizes examples of the refined ground truth in which minor branches were additionally annotated. On average, annotating and reviewing each image required approximately 20 minutes, totaling about 65 hours of expert effort for the 196 images. Figure 3 illustrates CAG-specific Copy-Paste augmentation and its modifications. Table 2 summarizes the segmentation performance of the models as measured by the three Dice metrics. Fine-tuned models substantially outperformed the pretrained baseline across all datasets. For $\text{Dice}_{\text{overall}}$, augmentation improved performance in every dataset, with the best result observed in ARCADE (69.09%, +3.25%). For $\text{Dice}_{\text{minor}}$, augmentation also provided consistent gains, and XCAD achieved the highest score (30.54%, +6.29%). XCAD already showed relatively strong performance before augmentation. In terms of relative improvement, DCA1 benefited most in $\text{Dice}_{\text{overall}}$ (+8.95%), while ARCADE showed the largest gain in $\text{Dice}_{\text{minor}}$ (+12.17%). For $\text{Dice}_{\text{major}}$, augmentation slightly decreased performance in ARCADE (−2.53%) and XCAD (−1.91%), while a modest gain was observed in DCA1 (+3.96%). Figure 4 shows qualitative segmentation results under $\text{Dice}_{\text{minor}}$, showing differences across datasets. The pretrained SAM-Med2D model showed the lowest performance, while fine-tuning with the DCA1, ARCADE, and XCAD datasets progressively improved the segmentation of minor arteries. Although conventional augmentation methods, such as rotation and flipping, showed slight performance improvements compared to simple fine-tuning, they did not exhibit substantial gains in terms of $\text{Dice}_{\text{minor}}$. Among them, the XCAD-trained model achieved the best results, and applying coronary-specific augmentation further enhanced performance compared with the non-augmented version.

To further assess the contribution of each augmentation component, we performed an ablation study using the DCA1 dataset (Table 3). Copy-Paste augmentation alone improved $\text{Dice}_{\text{overall}}$ from 55.29% to 59.98% and $\text{Dice}_{\text{minor}}$ from 13.89% to 17.88%. Adding intensity matching (`Intensity`), anatomical overlap (`Overlap`), or branching complexity (`Complexity`) provided additional gains. When two modifications were combined, the performance exceeded that of applying a single modification. The combination of all three achieved the highest scores ($\text{Dice}_{\text{overall}}$ 64.24%, $\text{Dice}_{\text{minor}}$ 24.19%). Overall, incremental improvements were observed with each step, and the best results were obtained when all components were applied together.

Discussion

The key finding of our study is that adding minor branch annotations to the test set substantially affected segmentation performance. The $\text{Dice}_{\text{minor}}$ was stricter than $\text{Dice}_{\text{overall}}$, consistently yielding lower scores and highlighting the difficulty of capturing thin and distal arteries. Fine-tuned models outperformed the pretrained baseline, particularly when trained with augmented data. Our augmentation strategy improved segmentation performance by up to 3.4-fold in $\text{Dice}_{\text{overall}}$ and 5.7-fold in $\text{Dice}_{\text{minor}}$ compared with the pretrained model. These findings underscore the challenge of segmenting thin and distal branches and the importance of tailored augmentation strategies for improving performance in these regions. While augmentation improved $\text{Dice}_{\text{minor}}$ and $\text{Dice}_{\text{overall}}$, $\text{Dice}_{\text{major}}$ showed a slight decrease in ARCADE and XCAD. This may suggest a trade-off,

as augmentations designed for minor epicardial artery delineation can introduce boundary variability, reducing accuracy in major epicardial arteries.

SAM-Med2D achieved Dice scores ranging from 57.16% to 87.69% in CT, MRI, endoscopy, and other modalities under the single-point prompt setting[24]. In CAG, however, its $\text{Dice}_{\text{overall}}$ was only 20.36%. Fine-tuning raised $\text{Dice}_{\text{overall}}$ to a level comparable with other benchmarks, but $\text{Dice}_{\text{minor}}$ remained low. This gap reflects both the imaging characteristics of CAG, such as small vessel caliber, overlapping structures, and low resolution, as well as the limited number of high-quality annotations for minor epicardial arteries. Expanding datasets by systematically labeling minor epicardial arteries may improve model performance.

The scarcity of public medical image datasets is a critical bottleneck for medical AI research[27]. Unlike natural image domains, where large-scale data are readily available, medical data are rarely shared openly. This limitation arises from legal, ethical, and societal imperatives to protect patient privacy[28]. Because clinical images and health records inherently contain sensitive information, broad disclosure is restricted unless they are thoroughly anonymized. To address this limitation, augmentation and synthesis are frequently employed in medical imaging research. Our study focused on augmentation specifically designed for CAG, whereas other groups have explored synthesis. For example, diffusion-based methods using CCTA-derived 2D projection masks have been applied to generate realistic angiographic images, and fractal synthetic modules have been introduced in self-supervised frameworks to create vessel-like masks that guide coronary angiogram generation[29,30].

Segmentation of pixel-width structures is one of the most difficult tasks in medical imaging. In coronary artery segmentation, these fine structures make accurate annotation both technically demanding and labor-intensive. Nevertheless, reliable ground truth annotations of these structures are essential for constructing dynamic coronary roadmaps and enabling advanced analyses of coronary blood flow[31,32]. They also provide a crucial reference for the development and thorough evaluation of AI methods in coronary imaging.

Future work may explore more advanced augmentation strategies. It may also involve expanding the scale of annotated datasets. Extending segmentation from images to videos can allow the use of temporal information in CAG. This study has several limitations. First, the Fine-ARCADE dataset was small in scale and limited to the right coronary artery. Annotation of the left coronary artery was not performed, which would have required substantially greater labeling effort and expert validation. In addition, external validation across broader multi-center cohorts was not performed, which restricts generalizability. Second, inter-observer variability was not formally assessed, which may cause annotation bias in the ground truth labels. Third, the analysis was confined to SAM-Med2D, without comparison to alternative architectures such as CNN-based models or other recently proposed foundation models. Finally, as previously mentioned, a slight performance decrease in $\text{Dice}_{\text{major}}$ was observed in XCAD and ARCADE compared to the performance improvement in $\text{Dice}_{\text{minor}}$. This could be attributed to two main reasons: the original main artery labeling being polygon-based rather than pixel-wise, potentially leading to inaccurate evaluation at boundary regions, and inaccurate predictions for thin line structures that are not actual blood vessels.

Conclusion

In this study, we developed a segmentation framework for CAG that includes refined annotations, specialized augmentation strategies, and a small-vessel-focused evaluation metric. Our approach substantially improved segmentation performance compared with the pretrained baseline, particularly in minor epicardial arteries. These results highlight the value of systematic labeling and specialized methods for advancing AI-based analysis of CAG.

References

1. Lawton, J. S. *et al.* 2021 acc/aha/scai guideline for coronary artery revascularization: a report of the american college of cardiology/american heart association joint committee on clinical practice guidelines. *Circulation* (2022).
2. Neumann, F. J. *et al.* 2018 esc/eacts guidelines on myocardial revascularization. *Eur Hear. J* (2019).
3. Kim, Y. I. *et al.* Artificial intelligence-based quantitative coronary angiography of major vessels using deep learning. *Int J Cardiol* (2024).
4. Sianos, G. *et al.* The syntax score: an angiographic tool grading the complexity of coronary artery disease. *EuroIntervention* (2005).
5. Suzuki, N. *et al.* Clinical expert consensus document on quantitative coronary angiography from the japanese association of cardiovascular intervention and therapeutics. *Cardiovasc. Interv Ther* (2020).
6. Collet, C. *et al.* Quantitative angiography methods for bifurcation lesions: a consensus statement update from the european bifurcation club. *EuroIntervention* (2017).
7. Witberg, G. *et al.* Diagnostic performance of angiogram-derived fractional flow reserve: a pooled analysis of 5 prospective cohort studies. *JACC Cardiovasc. Interv* (2020).

8. Xu, B. *et al.* Diagnostic accuracy of angiography-based quantitative flow ratio measurements for online assessment of coronary stenosis (favor ii china study). *J Am Coll Cardiol* (2017).

9. Avram, R. *et al.* Cathai: fully automated coronary angiography interpretation and stenosis estimation. *NPJ Digit. Med* (2023).

10. Labrecque Langlais, É. *et al.* Evaluation of stenoses using ai video models applied to coronary angiography. *NPJ digital medicine* (2024).

11. Kim, D. H. *et al.* Validation of artificial intelligence-based quantitative coronary angiography. *Digit. Heal.* (2024).

12. Yaman, S. Deep learning techniques for automated coronary artery segmentation and coronary artery disease detection: a systematic review of the last decade (2013–2024). *Int J Comput. Assist. Radiol Surg* (2025).

13. Yang, J. *et al.* Arcade: a large-scale coronary angiography dataset for stenosis detection and anatomical segmentation. In *MICCAI Workshop* (2023).

14. Li, Y. *et al.* Xcad: a coronary x-ray angiography dataset for vessel segmentation and stenosis detection. *Sci Data* (2023).

15. Ma, Y. *et al.* Dca1: a digital coronary angiography dataset for vessel segmentation. *Data Brief* (2022).

16. Camici, P. G. & Crea, F. Coronary microvascular dysfunction. *N Engl J Med* (2007).

17. Huo, Y. *et al.* Optimal diameter of diseased bifurcation segment: a practical rule for percutaneous coronary intervention. *EuroIntervention* (2012).

18. Starodumov, I. O. *et al.* Modelling of hemodynamics in bifurcation lesions of coronary arteries before and after myocardial revascularization. *Philos Trans A Math Phys Eng Sci* (2022).

19. Taqueti, V. R. & Di Carli, M. F. Coronary microvascular disease: pathogenic mechanisms and therapeutic options: Jacc state-of-the-art review. *J Am Coll Cardiol* (2018).

20. Kirillov, A. *et al.* Segment anything. In *Proceedings of the IEEE/CVF International Conference on Computer Vision (ICCV)* (2023).

21. Ma, J. *et al.* Segment anything in medical images. *Nat Commun* (2024).

22. Wu, J. *et al.* Medical sam adapter: adapting segment anything model for medical image segmentation. *Med Image Anal* (2025).

23. Zhang, K. & Liu, D. Customized segment anything model for medical image segmentation. *arXiv preprint arXiv:2304.13785* (2023).

24. Cheng, D. *et al.* Sam on medical images: a comprehensive study on three prompt modes. *arXiv preprint arXiv:2305.00035* (2023).

25. Ghiasi, G. *et al.* Simple copy-paste is a strong data augmentation method for instance segmentation. In *CVPR* (2021).

26. Finet, G. *et al.* Fractal geometry of arterial coronary bifurcations: a quantitative coronary angiography and intravascular ultrasound analysis. *EuroIntervention* (2008).

27. Tajbakhsh, N. *et al.* Embracing imperfect datasets: a review of deep learning solutions for medical image segmentation. *Med Image Anal* (2020).

28. Li, J., Li, W., Wang, Q., Wang, B. & Chen, H. A systematic collection of medical image datasets for deep learning. *ACM Comput. Surv* (2023).

29. Zhao, L., Zhang, H., Chen, X., Wang, Y. & Li, J. Leveraging diffusion model and image foundation model for improved correspondence matching in coronary angiography. *arXiv preprint arXiv:2504.00191* (2025).

30. Ma, Y. *et al.* Self-supervised vessel segmentation via adversarial learning. In *ICCV* (2021).

31. Piayda, K. *et al.* Dynamic coronary roadmap in percutaneous coronary intervention: results from an open-label, randomized trial. *Circ Cardiovasc. Interv* (2021).

32. Westra, J. *et al.* Diagnostic performance of in-procedure angiography-derived quantitative flow reserve compared to pressure-derived fractional flow reserve: the favor ii europe-japan study. *J Am Hear. Assoc* (2018).

Figure legends

Figure 1. **Overview of the Proposed Framework and Contributions.** Our framework consists of three key components: (1) **Fine-labeled Evaluation Dataset (Fine-ARCADE)** creation via expert annotation of minor vessels. (2) **CAG-specific Copy-Paste Augmentation** applied to coarse-labeled datasets for robust model training. (3) **Vessel Size-Specific Evaluation Metrics** ($\text{Dice}_{\text{overall}}$, $\text{Dice}_{\text{minor}}$, $\text{Dice}_{\text{major}}$) for granular performance analysis, particularly focusing on small-vessel detection.
Figure 2. **Refined ground truth in the Fine-ARCADE** Original coarse annotations, derived from the SYNTAX score and covering primarily major vessels, are shown in blue. In contrast, our newly refined annotations meticulously delineate the minor epicardial arteries, which are shown in red.
Figure 3. **Visualization of CAG-specific Copy-Paste augmentation** a) Background images and masks (yellow arrows). b) Foreground images and masks after geometric transformation (red arrows), with intensity distribution matched to the background images. c) Augmented images created by pasting b) onto a), generating anatomically continuous and morphologically diverse training datasets.
Figure 4. **Qualitative comparison of vessel segmentation results.** The figure illustrates the performance of models trained on different datasets and methods on two representative CAG images. The first two columns show the original image and the ground truth (major vessel in green, minor in yellow). Subsequent columns compare segmentation masks: Black represents correctly identified major vessels, blue for correctly identified minor vessels (True Positives), red for incorrect predictions (False Positives), and gray for unidentified minor vessels (False Negatives). The results clearly demonstrate that the proposed method, XCAD (Ours), achieves **Enhanced Minor Artery Detection** (highlighted in the zoomed box and red ellipses) by showing more blue region and significantly less red/gray region compared to the baseline XCAD (w/o aug.) and other methods, validating the effectiveness of our augmentation strategy.

Author contributions statement

Conceptualization: D.K, S.M.; Methodology: S.M and D.K.; Software and engineering: S.M, D.C, and D.K.; Resources: D.K, S.M, D.C, J.S, S.K, J.L, D.K, and J.M.; Data curation: D.K, J.S, S.K, and J.L.; Writing original draft: D.K, S.M.; Writing review & editing: D.K, S.M, and S.K.; Funding acquisition: D.K, and S.K.; Supervision: S.M and S.K.

Data availability

Public CAG dataset mentioned on our research is available at https://zenodo.org/records/10390295, https://github.com/AISIGSJTU/SSVS, and http://personal.cimat.mx:8181/~ivan.cruz/DB_Angiograms.html. Fine-ARCADE dataset is available at https://github.com/msw6468/CAGSAM.

Code availability

Source code of data preparation, augmentation, fine-tuning and evaluating SAMMed-2D is available at https://github.com/msw6468/CAGSAM.

Additional information

Ethical consent

The use of institutional data was approved by the Public Institutional Review Board (P01-202505-01-042), with the requirement for informed consent wavied.

Funding

This research was supported by the Bio&Medical Technology Development Program of the National Research Foundation (NRF) funded by the Korean government (MSIT) (no. RS-2025-00517929).

Competing interests

No potential conflict of interest relevant to this article was reported.

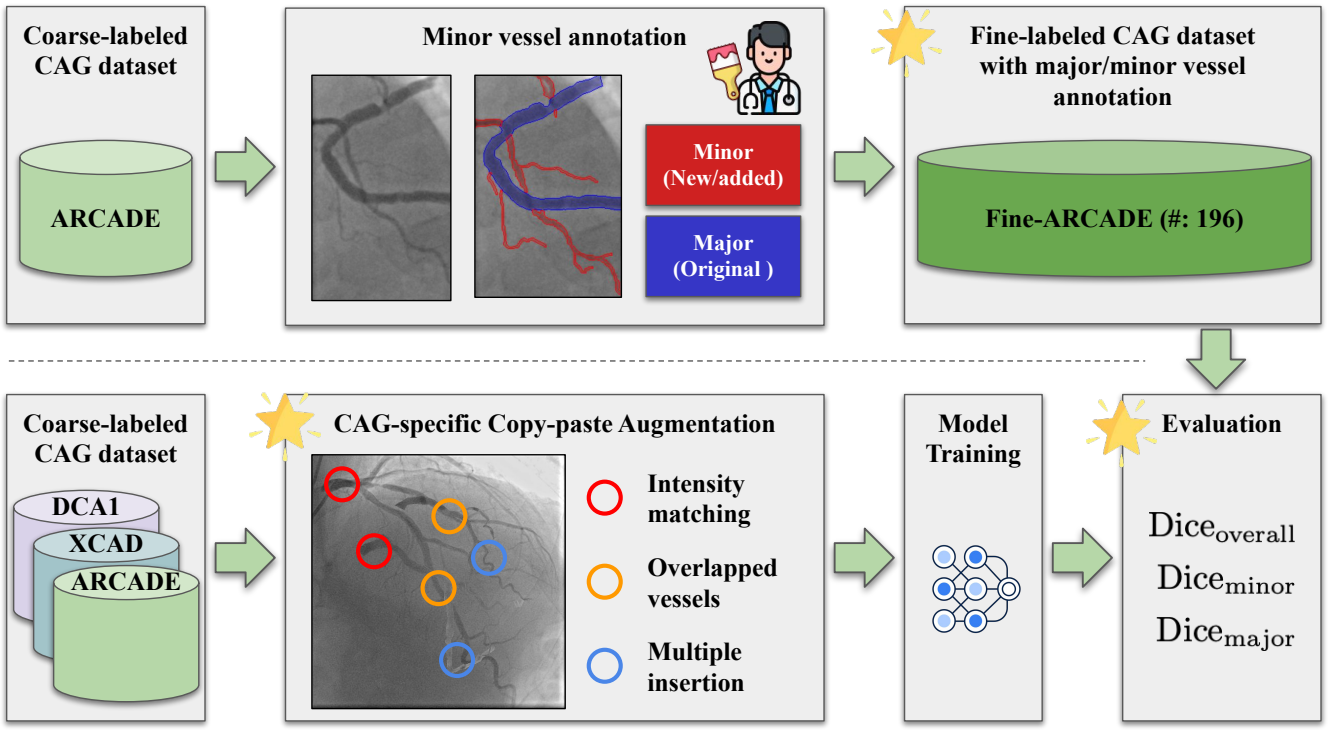

Figure 1. Overview of the Proposed Framework and Contributions. Our framework consists of three key components: (1) **Fine-labeled Evaluation Dataset (Fine-ARCADE)** creation via expert annotation of minor vessels. (2) **CAG-specific Copy-Paste Augmentation** applied to coarse-labeled datasets for robust model training. (3) **Vessel Size-Specific Evaluation Metrics** ($\text{Dice}_{\text{overall}}$, $\text{Dice}_{\text{minor}}$, $\text{Dice}_{\text{major}}$) for granular performance analysis, particularly focusing on small-vessel detection.

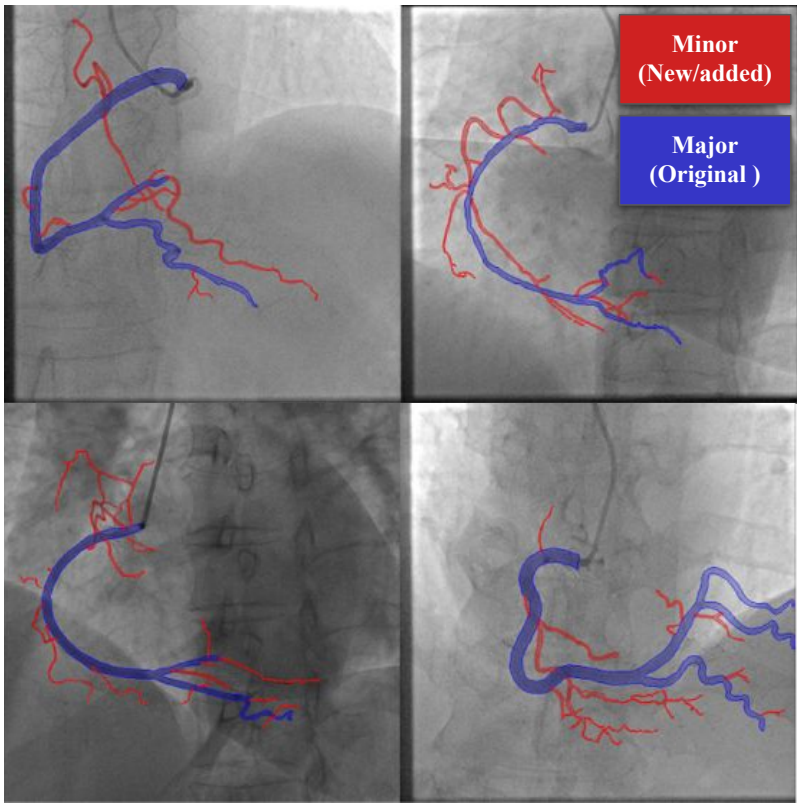

Figure 2. Refined ground truth in the Fine-ARCADE Original coarse annotations, derived from the SYNTAX score and covering primarily major vessels, are shown in blue. In contrast, our newly refined annotations meticulously delineate the minor epicardial arteries, which are shown in red.

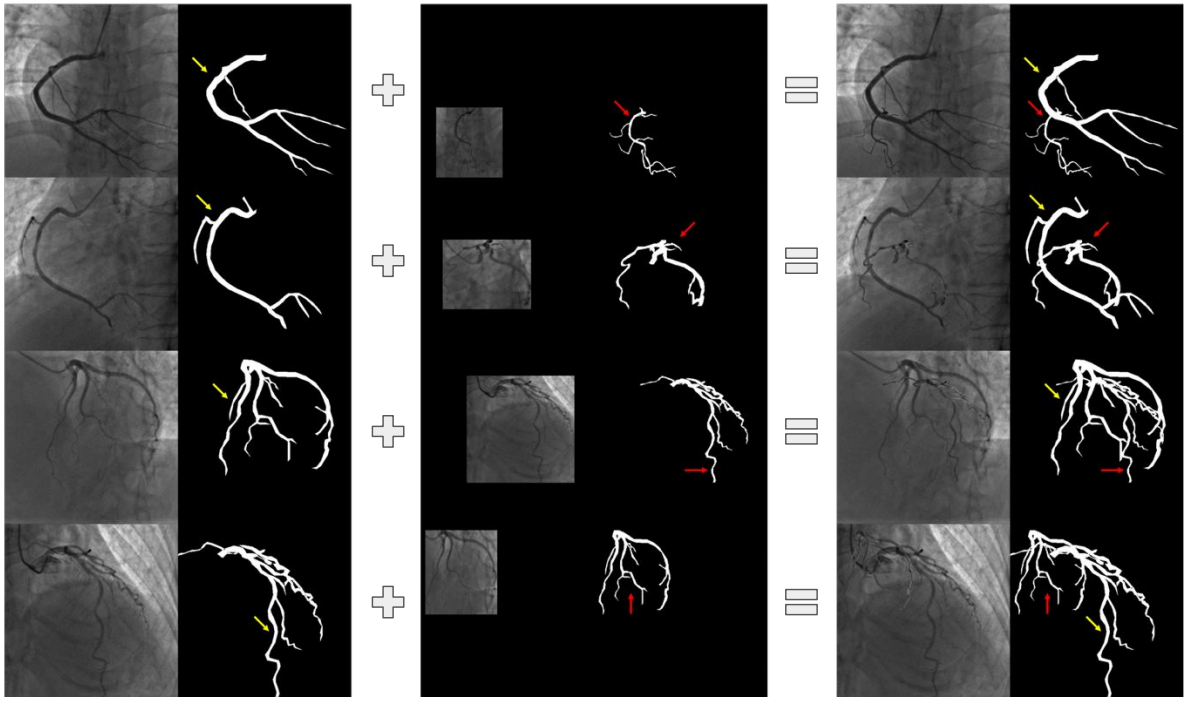

Figure 3. Visualization of CAG-specific Copy-Paste augmetation a) Background images and masks (yellow arrows). b) Forground images and masks after geometric transformation (red arrows), with intensity distribution matched to the background images. c) Augmented images created by pasting b) onto a), generating anatomically continuous and morphologically diverse training datasets.

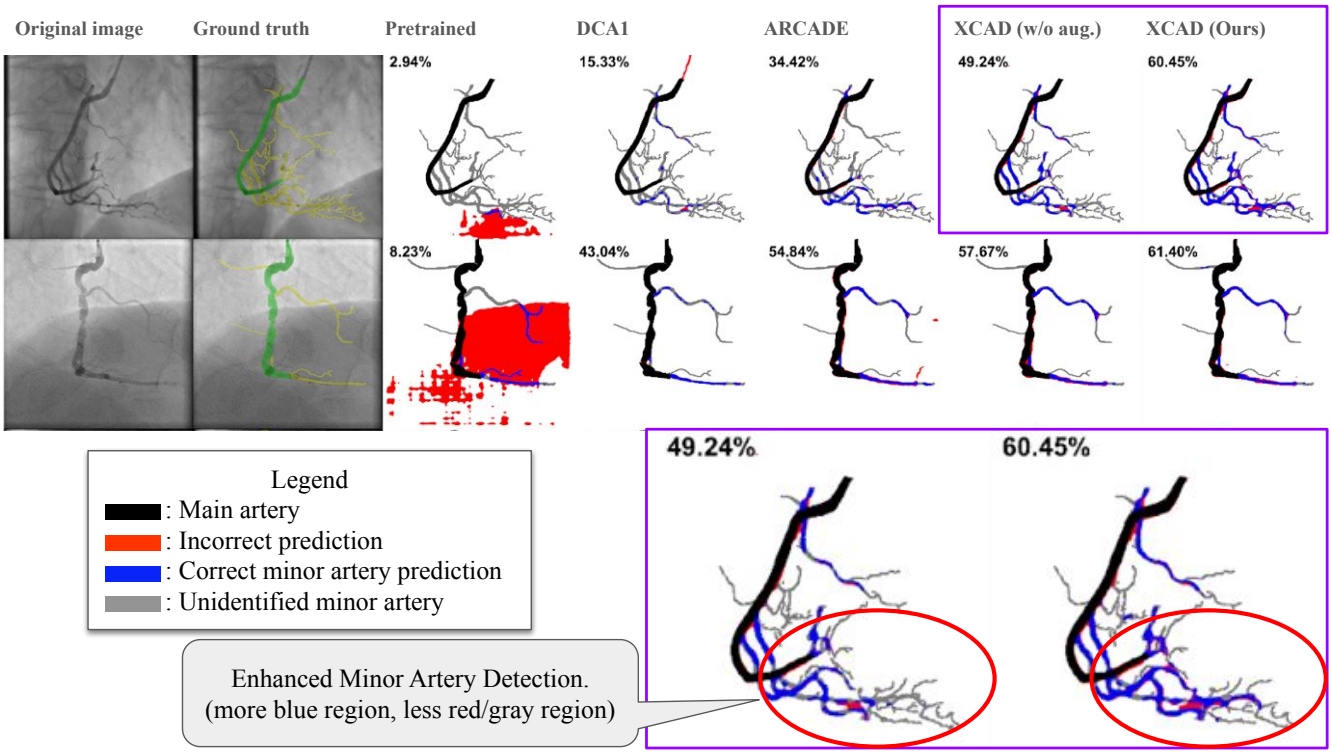

Figure 4. Qualitative comparison of vessel segmentation results. The figure illustrates the performance of models trained on different datasets and methods on two representative CAG images. The first two columns show the original image and the ground truth (major vessel in green, minor in yellow). Subsequent columns compare segmentation masks: Black represents correctly identified major vessels, blue for correctly identified minor vessels (True Positives), red for incorrect predictions (False Positives), and gray for unidentified minor vessels (False Negatives). The results clearly demonstrate that the proposed method, XCAD (Ours), achieves **Enhanced Minor Artery Detection** (highlighted in the zoomed box and red ellipses) by showing more blue region and significantly less red/gray region compared to the baseline XCAD (w/o aug.) and other methods, validating the effectiveness of our augmentation strategy.

Table 1. Public datasets for CAG segmentation.

Dataset	Size	Resolution	Minor artery	Details
ARCADE[13]	1500	512×512	$\times$	labeled by experts based on the SYNTAX score
XCAD[14]	126	512×512	$\times$	labeled by experienced radiologists
DCA1[15]	130	300×300	$\times$	labeled by an expert cardiologist
Fine-ARCADE (Ours)	196	512×512	$\circ$	Segmentation mask of RCA with minor arteries (based on ARCADE)

Table 2. Model performance using conventional and newly proposed metrics, based on ground truth including minor branches.

Dataset	Method	$\text{Dice}_{\text{overall}}$	$\text{Dice}_{\text{minor}}$	$\text{Dice}_{\text{major}}$
-	Pretrained	20.36	5.37	24.89
ARCADE	Fine-tune	65.84	12.04	82.35
	Flip	65.89	12.60	82.49
	Rotation	67.20	12.36	**83.91**
	Ours	**69.09**	**24.21**	79.82
XCAD	Fine-tune	64.63	24.25	75.84
	Flip	65.00	25.33	75.74
	Rotation	66.58	25.87	**77.68**
	Ours	**67.68**	**30.54**	73.93
DCA1	Fine-tune	55.29	13.89	68.70
	Flip	55.37	12.74	69.27
	Rotation	57.03	15.26	70.30
	Ours	**64.24**	**24.19**	**72.66**

Table 3. Ablation study of CAG-specific Copy-Paste augmentation on DCA1 dataset.

Copy-Paste	Intensity mathching	Overlap vessels	Multiple insertion	$\text{Dice}_{\text{overall}}$	$\text{Dice}_{\text{minor}}$	$\text{Dice}_{\text{major}}$
×	×	×	×	55.29	13.89	68.70
○	×	×	×	59.98	17.88	72.07
○	○	×	×	61.46	19.42	72.93
○	×	○	×	62.31	21.07	72.52
○	×	×	○	62.59	19.47	**73.92**
○	○	×	○	62.94	20.95	72.58
○	×	○	○	63.22	22.52	72.72
○	○	○	×	63.40	23.84	71.74
○	○	○	○	**64.24**	**24.19**	72.66